Multispectroscopic and molecular modeling studies on the interaction of two curcuminoids with β-lactoglobulin

F. Mohammadi, Mehdi Sahihi, A. Khalegh Bordbar

Multispectroscopic and molecular modeling studies on the interaction of two curcuminoids with β-lactoglobulin

F. Mohammadi [a b], M. Sahihi [a], A. Khalegh Bordbar [a]

[a] Department of Chemistry, University of Isfahan, Isfahan 81746-73441, Iran

[b] Department of Chemistry, Institute for Advanced Studies in Basic Sciences (IASBS), Gava Zang, Zanjan 45137-66731, Iran

Abstract

This study demonstrates the binding properties of bisdemethoxycurcumin (BDMC) and diacetylbisdemethoxycurcumin (DABC) as bioactive curcuminoids with bovine β-lactoglobulin (BLG) variant B using fluorescence and circular dichroism (CD) spectroscopy; molecular docking, and molecular dynamics simulation methods. The estimated binding constants for BLG-BDMC and BLG-DABC complexes were $(8.99 \pm 0.10) \times 10^4\ M^{-1}$ and $(1.87 \pm 0.10) \times 10^2\ M^{-1}$, respectively. The distances between BLG and these curcuminoids were obtained based on the Förster's theory of non-radiative energy transfer. Molecular docking studies revealed the binding of BDMC and DABC to the protein surface cleft of protein by formation of four and one hydrogen bonds, respectively. Finally, molecular dynamics simulation results represent the conformational changes of BLG due to its interaction with BDMC. Also, the profiles of atomic fluctuations signified the rigidity of ligand binding site during the simulation.

Keywords

Curcuminoids

Bovine β-lactoglobulin

Fluorescence

Circular dichroism

Molecular dynamics simulation

Introduction

The lipocalin superfamily consists of small secreted proteins that typically bind and transfer small hydrophobic ligands and interact with cell-surface receptors [1], [2]. The bovine β-lactoglobulin (BLG) as one of the natural lipocalin member, is the major bovine whey protein and has several genetic variants that among them phenotypes A and B are the most predominant [3], [4]. The crystal structure shows that the 162 amino acids along single polypeptide chain of bovine BLG form a calyx composed of an eight-stranded antiparallel β-sheet [5]. The significant physico-chemical property of this lipocalin protein is its ability to bind *in vitro* several physiologically relevant ligands such as steroids, fatty acids, retinoids, vitamin D, and cholesterol [6], [7], [8]. Therefore, BLG can serve as a potent carrier, especially for poor water-soluble molecules.

Curcumin (CUR), [1,7-bis(4-hydroxy-3-methoxyphenyl)1,6-heptadiene-3,5-dione] (Scheme 1a) and bisdemethoxycurcumin (BDMC) (Scheme 1b), isolated from the roots of the *Curcuma longa* Linn (commonly known as turmeric), have been shown to regulate a number of biological responses [9], [10], [11], [12], [13]. It has been shown that curcuminoids display anticarcinogenic [14], [15], antioxidant [16], [17], anti-inflammation [18], anti-angiogenic properties [19], [20]. Moreover, the modulation of multi-drug-resistance gene and protein function by curcuminoids were also reported [21], [22]. The antimetastasis [23], antitumor and antioxidant activity of BDMC are much greater than CUR [24], [25], [26]. It has been also shown that BDMC is the most potent and selective inhibitor and represents a promising lead for the development of more potent and specific agents targeting AKR1B10 as a human member of the aldo–keto reductase (AKR) superfamily [27]. Diacetylbisdemethoxycurcumin (DABC) (Scheme 1c) is a new synthetic acetylated derivative of CUR and has been also shown to display moderate cytotoxicity (IC_{50} ~10 μM) [28].

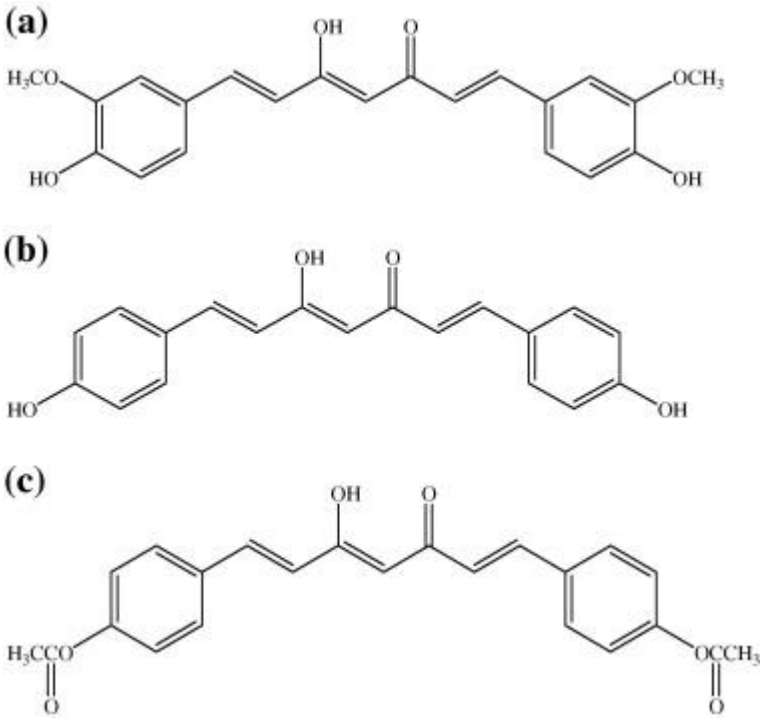

Scheme 1. Chemical structure of curcumin (a), bisdemethoxycurcumin (BDMC) (b) and diacetylbisdemethoxycurcumin (DABC) (c).

One of the main limitation of the curcuminoids for biomedical application refers to their poor solubility and consequently, low bioavailability. This inadequacy could be removed by loading of these bioactive compounds in carrier proteins. In our previous studies, the ability of serum albumins and beta-casein for transporting of these bioactive compounds were investigated by exploring the binding mechanism [29], [30], [31]. In the present study, the interaction of BDMC and DABC with BLG have been comprehensively investigated by using various spectroscopic and molecular modeling methods in order to explore the binding properties of these systems and evaluating the capability of BLG to transport these curcuminoids.

Experimental

Materials

Bovine BLG type B was purchased from Sigma Chemical Company. BDMC was separated from curcumin and DABC was synthesized based on previous method [28]. Ethanol was obtained from

Merck Company. All other materials and reagents were of analytical grade. Double distilled water was used for preparing the buffer solution.

Preparation of BLG solution

For spectroscopic sample preparation, BLG was weighed and dissolved in 0.05 M, pH 6.4 phosphate buffer solution. The exact concentration of protein was determined spectrophotometrically using molecular absorption coefficient of ε_{278nm} = 17,600 M^{-1} cm^{-1} [32].

Preparation of BDMC and DABC solutions

The stock solutions of the curcuminoids were prepared by dissolving BDMC and DABC in ethanol. The required diluted solutions in buffer were made from these stock solutions and their UV–Vis absorption spectra were recorded between 250 and 600 nm. From the absorption versus concentration graph at the λ_{max} point (using the Beer–Lambert law), the molar absorption coefficient of BDMC at 417 nm and DABC at 396 nm were found to be 46,193 and 19,122 M^{-1} cm^{-1}, respectively.

Fluorescence measurements

BLG solution (3 mL, 4 μM) in a 0.05 M, pH 6.4 phosphate buffer was prepared in a 1 cm rectangular cell. The BDMC and DABC solutions (1 mM) were consecutively added in μL volumes using trace Eppendorf pipette to the cell placed in the sample chamber of spectrofluorimeter (Cary, Eclips, Varian Co., Australia). The excitation and emission slit widths were set at 10 and 5 nm, respectively. The excitation wavelength was adjusted at 295 nm to selectively excite the tryptophan residues of BLG. The emission spectra were recorded for all of the samples in the range of 300–450 nm at 25 °C with a scan speed of 150 nm/min. Integration of spectra was done in the range of 300–400 nm to obtain the peak area. During the fluorescence measurements, ethanol content that was added with ligand to the protein solution never exceeded 3% (v/v). Control experiment was done on BLG with ethanol and proved the negligible effect of ethanol on the fluorescence intensity of BLG. The other control experiments for evaluating any inner filtering were also carried out and proved that inner filter effect corrections are not required for the fluorescence data.

Circular dichroism measurements

All the circular dichroism (CD) spectra were recorded using Aviv spectropolarimeter model 215 (Proterion Corp., USA) at 25 °C. The scan speed was 20 nm min^{-1} and each spectrum was the average of three accumulated spectra. The CD spectra were recorded in the far-UV region (190–260 nm) using 1 mm path length cell. The far-UV CD spectra were used to investigate the changes in the secondary structure of BLG. The protein concentration in the experiments for far-UV region was 13.6 μM and the results were expressed in molar ellipticity [θ] (deg cm^2 $dmol^{-1}$). The CDNN software was used to predict the secondary structure of the protein according to the statistical method [33], [34]. During the CD spectroscopic measurements, ethanol content in the solutions never exceeded 1.5% (v/v). By applying Fourier transform infrared spectroscopy, Dufour et al. have shown that the secondary structure of BLG is unaffected by ethanol up to ∼20% (v/v) [35], hence, with respect to the ethanol concentration in our CD measurements, ethanol should have no considerable effect on the secondary structure of BLG. However, the control experiment was done to evaluate the effect of ethanol up to 1.5% (v/v) content on the CD spectra of BLG and no considerable changes reflecting the ethanol effect were observed.

Molecular docking

The molecular docking program ArgusLab 4.0.1 [36] was employed for finding out the most stable conformations of BDMC-BLG and DABC-BLG complexes. Earlier ArgusLab 4.0.1 validation studies have reported very little difference in the docking accuracies between ArgusLab and Genetic optimization for ligand docking (GOLD) [36], [37], [38]. However, the accuracy of ArgusLab was checked by redocking the dodecyl sulfate to BLG. After docking the dodecyl sulfate back into BLG, The RMSD value between docked dodecyl sulfate and BLG were similar to those of original modes, suggesting that ArgusLab is suitable for docking of ligands to BLG. In the docking calculations, the scoring method Ascore from the ArgusLab 4.0.1 suite is employed. Ascore is based on the decomposition of the total protein–ligand binding free energy, taking into account the following contributions: the van der Waals interaction between the ligand and the protein, the hydrophobic effect, the hydrogen bonding between the ligand and the protein, the hydrogen bonding involving charged donor and/or acceptor groups, the deformation effect, and the effects of the translational and rotational entropy loss in the binding process, respectively [36], [37].

Preparation of the protein and the ligand

The known crystal structure of BLG (PDB ID: 3NPO) was obtained from the RCSB Protein Data Bank and water molecules were removed. In order to get the most stable conformations of BDMC and DABC, the structure-optimizing calculations were carried out at the 6-31G** level by employing the Becke three-parameter Lee–Yang–Parr (B3LYP) hybrid density functional theory using the quantum chemistry software GAMESS [39]. ArgusDock exhaustive search docking engine was used which had the grid resolution of 0.40 Å. Docking precision was set to high precision. To recognize the binding sites on BLG, blind dockings were carried out and the grid size was set to 146 Å, 156 Å, and 132 Å along the *X*, *Y*, and *Z* axes, respectively.

MD simulations

MD simulations of the BLG, BLG-BDMC and BLG-DABC complexes in explicit water were carried out using the GROMACS 4.5.6 package [40], [41] and the GROMOS96 43a1 force field [42], [43] for a time scale of 10,000 ps. Three dimensional periodic boundary conditions were imposed, enclosing the molecule in a cubic box (6.65049 × 6.65049 × 6.65049 nm^3) solvated with the SPC water model [44] provided in the GROMACS package. The distance between the grid box and the protein and/or protein–ligand complex was set to 1.0 nm. The system was neutralized with 8 Na^+ counterions. The topology parameters of BLG were created using the Gromacs program. The topology parameters of BDMC and DABC were built by the Dundee PRODRG2.5 server (beta) [45]. The partial atomic charges of the ligand molecules were subsequently determined by using the GAMESS [39] at the level of HF/6-31G**. Firstly, the steepest decent energy minimization for 2000 steps was performed to release conflicting contacts. Then a 60 ps position-restrained simulation was performed by keeping the coordinates fixed at 300 K to allow the relaxation of solvent molecules. Finally, a 10,000 ps dynamic simulation was submitted at 300 K temperature and 1 bar pressure. The electrostatic terms were described using the particle mesh Ewald algorithm and the motion equations were integrated by applying the leaf-frog algorithm with a time step of 2 fs. The atomic coordinates were recorded every 0.5 ps during the simulation for the latter analysis.

Results and discussion

Fluorescence studies of BLG quenched by BDMC and DABC

Fluorescence quenching measurement is one of the widely used techniques in the field of ligand–protein interaction. This method can reveal the accessibility of quenchers to the fluorophores of protein, help to understand the binding mechanism and provide clues to the nature of the binding phenomenon. In principle both the fluorescence of native protein and the fluorescence of ligand (if any) can be exploited to monitor the complex formation. However, most of the studies rely on the quenching of protein fluorescence. Monitoring quenching of tryptophan fluorescence in comparison of monitoring increases in ligand fluorescence, yields much better signal to noise ratio. Fluorescence quenching could proceed through different mechanisms, usually classified as dynamic and static quenching. Static quenching refers to the formation of a non-fluorescent ground state complex, whereas, dynamic quenching is resulted from the collision encounter between the fluorophore and quencher. Moreover, energy transfer, excited state reactions and molecular rearrangement could also be accounted as other mechanisms of fluorescence quenching.

Both static and dynamic processes are described by the Stern–Volmer equation as follows [46]:

$$\frac{F_0}{F} = 1 + k_Q \tau_0 [Q] = 1 + K_{SV} [Q] \quad (1)$$

In this equation, F_0 and F are the fluorescence intensities in the absence and presence of quencher, [Q] is the quencher concentration and K_{SV} is the Stern–Volmer quenching constant, which should be equal to $k_Q \tau_0$, where k_Q and τ_0 are the bimolecular quenching rate constant and the average lifetime of the biomolecule without quencher (τ_0 ~1.45 ns for BLG in pH 6.4 [47]), respectively. The concentration of quencher should be the free concentration, but in our analysis, the total concentration of ligands (BDMC and DABC) were used. When the ligand concentration is in excess of available for specific protein binding sites, this approximation is valid. The total intensity of fluorescence emission is usually expressed by the peak height, but it is more reasonable to use the total area of fluorescence emission. Hence, in the present study, we applied the peak area of protein fluorescence spectra without (S_0) or with (S) ligand, instead of F_0 and F in the Stern–Volmer equation.

The fluorescence spectra of BLG in the presence of different concentrations of BDMC and DABC were shown in Fig. 1. The fluorescence intensity of BLG gradually decreased with increasing the

concentration of both curcuminoids; in the meanwhile, the maximum emission wavelength did not show any red or blue shift. Thus, it indicates the formation of BLG–ligand complex. The BLG intrinsic fluorescence is referred to the two tryptophan residues in the position 19 and 61. According to the structural models, the indole group of Trp-19 is at the bottom of the central hydrophobic calyx of the protein, while Trp-61 is a part of an external loop and close to Cys160–Cys66 disulfide bond. The water accessibility of Trp-19 is, accordingly, much lower than Trp-61 [48], [49], [50]. Cho et al. showed that the intrinsic fluorescence was substantially diminished in genetically modified Trp-19 to Ala-19, demonstrating that Trp-61 was a minor contributor to overall fluorescence emission of BLG [51]. This can be due to the location of Trp-61 near a disulfide bond (Cys66–Cys160) or near the guanidine group of Arg-124 (3–4 Å distance from Trp-19 indole ring [5]), which can quench its emission, and/or to the self-quenching of Trp-61 of the other monomer in the BLG dimer form [48], [49].

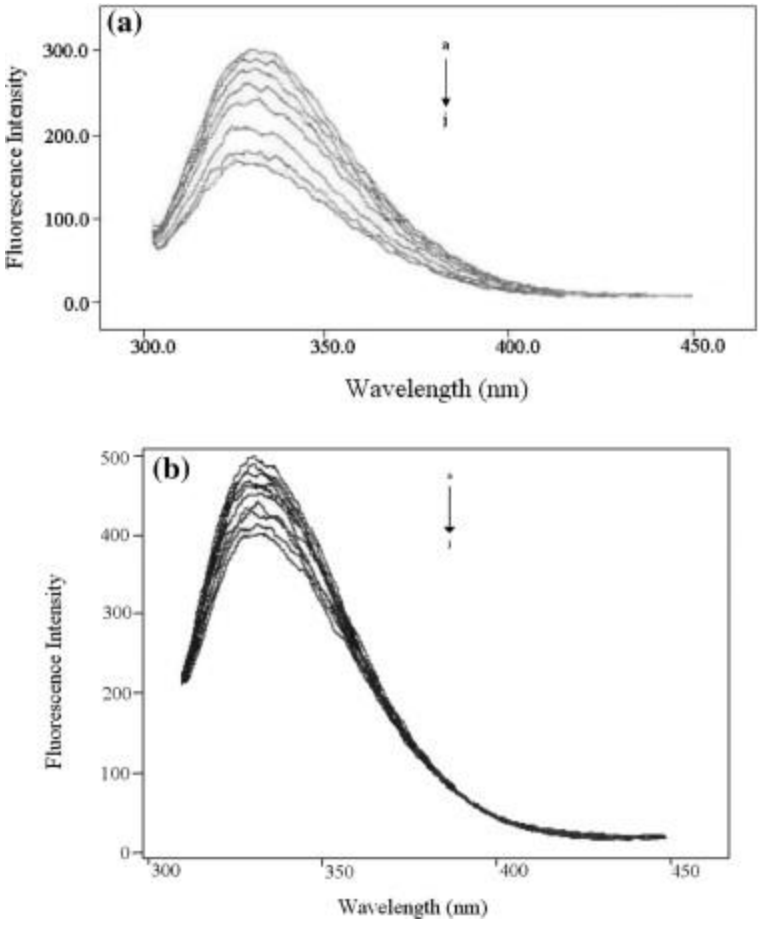

Fig. 1. The Fluorescence spectra of BLG (4 μM) at different concentrations of BDMC (a) and DABC (b): 0 μM(a), 2.2 μM (b), 5.5 μM (c), 9.1 μM (d), 13.5 μM (e), 23.8 μM (f), 32.9 μM (g),

39.8 μM (h), 48.6 μM (i) and 57.2 μM (j) measured in 0.050 M phosphate buffer pH 6.4, λ_{ex} = 295 nm.

The estimated K_{SV} and k_Q values from the plot of S_0/S versus the ligand concentration are listed in Table 1. Diffusion-controlled quenching typically results in values of k_Q close to 2×10^{10} M^{-1} s^{-1} [52]. The values of k_Q which are smaller than the diffusion-controlled value can be related to the steric shielding of the fluorophore or a low quenching efficiency. The apparent value of k_Q which is larger than the diffusion-controlled limit usually indicates some type of binding reaction. In the present case, the values of k_Q are larger than the diffusion-controlled limit. Hence, both curcuminoids should be bound to BLG and the main mechanism of quenching is not dynamic.

Table 1. The Stern–Volmer constant K_{SV}, biomolecular quenching rate constant k_Q, number of substantive binding sites n and the binding constant K_A for interaction of BDMC and DABC with BSA obtained from the fluorescence quenching measured in 0.050 M phosphate buffer, pH 6.4 at λ_{ex} = 295 nm and [BLG] = 4 μM.

Empty Cell	**BDMC**	**DABC**
K_{SV} (M^{-1})	1.78×10^4	3.81×10^3
k_Q (M^{-1} s^{-1})	1.23×10^{13}	2.63×10^{12}
n	1.15	0.71
K_A (M^{-1})	8.99×10^4	1.87×10^2
$\Delta G°$ (kcal mol^{-1})	6.75	3.10

By assuming the static fluorescence quenching of protein and the existence of *n* substantive binding sites on protein to accommodate the ligand molecules, the equilibrium between free and bound molecules could be given by the following equation [53]:

$$\ln\frac{F_0-F}{F} = \ln K_A + n\ln[Q] \quad (2)$$

where F_0, F and [Q] are the same as the parameters in the Stern–Volmer equation. K_A is the apparent binding constant reflecting the reaction extent between protein and ligand. Similar to the Stern–Volmer plot, the peak areas were used instead of fluorescence intensity in Eq. (2). The estimated values of K_A and n from the intercept and slope of the plots of $\ln(S_0/(S-1))$ versus ln[Q] are listed in Table 1. A single binding site system can be figure out from the n values. The obvious difference between the K_A values indicates the higher affinity of BDMC than DABC to bind to BLG. The results of our previous study also revealed the great different binding affinities of BDMC and DABC toward HSA [31]. Hence, the significant role of the phenolic OH groups in the structure of BDMC which are acetylated in DABC can be confirmed in the binding process. These results were fully supported by the computational calculations (see Section 'Molecular docking studies').

Our recent studies on the binding affinities of both natural, (e.g. CUR and BDMC), and synthetic, (e.g. DAC and DABC) curcuminoids with proteins like HSA, BSA, and BLG have demonstrated that highest binding affinity from among them is exhibited by CUR, and the lowest by the DABC [31], [54], [55]. The findings have helped us in developing an understanding on the role of functional groups of curcuminoids and the nature of the forces involved in the interactions. CUR was shown to exhibit higher affinity than DAC for binding to BLG and also serum albumins (HSA and BSA) [54], [55]. It indicates that the phenolic hydroxyl groups have a major role to play in their interactions with the proteins. The role of phenolic OH groups is further confirmed by our results on BDMC and DABC interactions with HSA [31]. Interactions of proteins with acetylated derivatives, like DAC and DABC, both of which are devoid of phenolic hydroxyl groups, exhibit lower binding affinity for DABC. It therefore suggests that methoxy groups on the curcuminoids also contribute to their interactions with the proteins. On the other hand, results of protein interaction with CUR and BDMC, both of which contain the phenolic OH groups, reveal nearly the same binding affinity. These results imply that the role of the phenolic hydroxyl groups in the

ascribed interactions is essentially more important than the methoxy groups which may be interpreted as a stronger interaction between the OH groups and the binding site. On the basis of the discussion on the involved functional groups, the hydrogen bonding through the phenolic OH groups may be the most determinant force in the ascribed interactions.

Energy transfer between BLG and BDMC

Fluorescence resonance energy transfer (FRET) is a non-destructive spectroscopic method that can estimate distance from the bound ligand to the fluorophore groups of macromolecule. The energy transfer could take place through direct electrodynamic interaction between the primarily excited molecule and its neighbors. The following conditions determine the occurrence of energy transfer between a donor and an acceptor: (i) the relative orientation of the donor and acceptor electric dipole moments; (ii) the overlap between the emission spectrum of the donor and the UV–Vis spectrum of the acceptor; and (iii) the distance between the donor and the acceptor [56].
According to the Förster's dipole–dipole non-radiative energy transfer theory, the efficiency of energy transfer (E) is related not only to the distance between the acceptor and the donor, but also to the critical energy transfer distance (R_0). As described by the following equation [46]:

$$E = 1 - \frac{F}{F_0} = \frac{R_0^6}{R_0^6 + r^6} \quad (3)$$

where F and F_0 are the fluorescence intensity of the donor in the absence and presence of equal amount of acceptor, r is the distance from the bound ligand to the tryptophan residue, and R_0 is the Förster critical distance at which 50% of the excitation energy is transferred to the acceptor and can be calculated by the following equation:

$$R_0^6 = 8.8 \times 10^{-2} K^2 N^{-4} \Phi J \quad (4)$$

where K^2 is a factor describing the relative orientation of the transition dipoles of the donor and acceptor (for a random orientation as in fluid, $K^2 = 2/3$), N is the average refractive index of the medium in the wavelength range where spectral overlap is significant, Φ is the fluorescence quantum yield of the donor, and overlap integral J expresses the extent of overlap between the normalized fluorescence emission spectrum of the donor and the acceptor absorption spectrum. J is given by the following equation:

$$J = \frac{\sum F(\lambda)\varepsilon(\lambda)\lambda^4 \Delta\lambda}{\sum F(\lambda)\Delta\lambda} \quad (5)$$

In this equation, $F(\lambda)$ is the fluorescence intensity of the fluorescent donor at wavelength λ and is dimensionless, $\varepsilon(\lambda)$ is the molar absorption coefficient of the acceptor at wavelength λ. In the present study, we prepared the solutions containing equimolar concentrations of ligand (BDMC or DABC) and BLG and the UV–Vis absorption spectra were recorded. As the fluorescence emission of protein is affected by the excitation light at 295 nm, the spectrum ranged from 300 to 500 nm was chosen to obtain the overlapping integral. The UV–Vis spectrum of DABC and BLG solution did not show considerable absorption in the wavelength range of 300–500 nm (data are not shown), so, the energy transfer calculation could not be calculated. As shown in Fig. 2, the overlapping between the fluorescence emission of free BLG and the absorption spectrum of BDMC is considerable. The efficiency of energy transfer and overlapping integration can be easily calculated using Eqs. (3), (5), respectively. For calculating the Förster critical distance in Eq. (4), K^2 is 2/3, N is 1.3598, and Φ is 0.08 [57]. By using the obtained value for R_0 from the Eq. (4) and E from the Eq. (3), the r value can be calculated. We could calculate that $J = 1.9358 \times 10^{-14}$ cm^3 M^{-1}, $R_0 = 2.535$ nm, $E = 0.169$, and $r = 3.307$ nm.

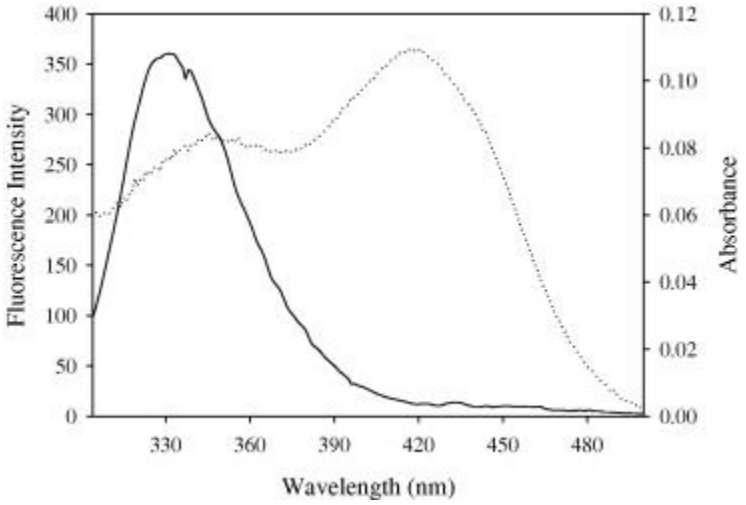

Fig. 2. Fluorescence emission (solid lines) and UV–Vis absorption (dotted lines) of solution containing BDMC and BLG measured in 0.050 M phosphate buffer pH 6.4 λ_{ex} = 295 nm and [BLG] = [BDMC] = 6 μM.

With respect to the structural dimensions of BLG ($3.8 \times 3.6 \times 3.4$ nm^3), the estimated r value from the FRET calculation is accompanied by a relatively large error and cannot demonstrate the distance from the bound BDMC to the tryptophan residues (Trp-19 and Trp-61). Hence, we applied the established method of Lange et al., to determine the binding site from the FRET measurement with the crystallographic coordinates of BLG [58]. The central calyx and the surface cleft have been proposed as two potential ligand binding sites of BLG for hydrophobic molecules. In the Lange method, the Lys-141 and Lys-70 are taken as reference points for the interior cavity and the surface cleft, respectively. The average distances from the tryptophan residues, Trp-19 and Trp-61, to the reference points of the potential binding pockets are determined from a crystallographic model of BLG (with resolution of 2.8 Å). Assuming either the surface cleft or the central cavity as alternative binding sites, we calculated the FRET efficiency, E^{theor} from the Eq. (3) as a function of the average distances (r) from the crystallographic model and the critical distance R_0 from the quenching experiment. The theoretical value of FRET efficiency, E^{theor}, assuming surface cleft and interior cavity was obtained to be 0.41 and 0.92, respectively. The comparison between these results and experimentally determined value of energy transfer efficiency, $E^{exp} = 0.169$, reveals that the surface cleft is more probable than the central calyx to be the binding site for BDMC. This result is confirmed by the computational calculations (see Section 'Molecular docking studies').

It is of worthy to mention that in the present experimental conditions including the buffer solution and pH (0.05 M phosphate buffer, pH 6.4), the stability of BDMC as a derivative of CUR has been significantly considered [59], [60]. On the other hand, BLG undergoes the Tanford transition as the reversible conformational transition occurring from pH 6.5 to 9.5 and is related to the descriptive open or closed calyx conformational structure of BLG. It has been observed that a loop segment between beta sheet E and F of BLG acts structurally like a lid to close the calyx site at pH 6.2 and open it at pH 7.1–8.2 [61]. Hence, it can be inferred that the central calyx of BLG at pH 6.4 is more likely in the closed state and the entrance of the BDMC molecule to this binding site is hindered. This conclusion can strengthen the assumption of the surface cleft as the binding site. These results represent that the hydrophobic interactions did not have a dominant role in the binding of BDMC to BLG. A similar situation has been recently observed for binding of resveratrol, serotonin and arachidonyl serotonin to BLG [62], [63].

Circular dichroism

Circular dichroism (CD) is one of the strong and sensitive spectroscopic techniques to explore the various aspects of protein structure and ligand–protein interactions. The far-UV region (190–250 nm) can be used to investigate the secondary structure contents of proteins. The main absorbing groups in this region are peptide bonds.

The CD spectrum of BLG is typical of a protein that is comprised of anti-parallel β-structure and shows a minimum at 217 nm. The far-UV circular dichroism spectrum of BLG in the absence and presence of BDMC and DABC at four ligand/protein (L/P) molar ratios (0, 0.25, 0.50 and 0.75) is shown in Fig. 3 and the corresponding secondary structure contents are listed in Table 2. The CD spectra of native BLG are consistent with those previously reported [62], [63]. According to Fig. 3a and Table 2, the α-helix content of BLG in the presence of BDMC has been increased, but the increasing trend is not regular and the increasing trend of α-helix content compensates with the decreasing trend of the random coil and the β-sheet contents. As can be seen from Fig. 3b and Table 2, the alteration in the secondary structure of BLG due to the interaction with DABC is not significant. It can be deduced that ligand-induced conformational changes are localized in the binding site and do not involve significant alterations in the folding and stability of BLG. However, the more detectable changes in the secondary structure contents of BLG in the presence of BDMC may reflect the stronger interaction with BDMC than DABC which is in consistent with the fluorescence quenching and molecular docking results (see Sections ‘Fluorescence studies of BLG quenched by BDMC and DABC’ and ‘Molecular docking studies’).

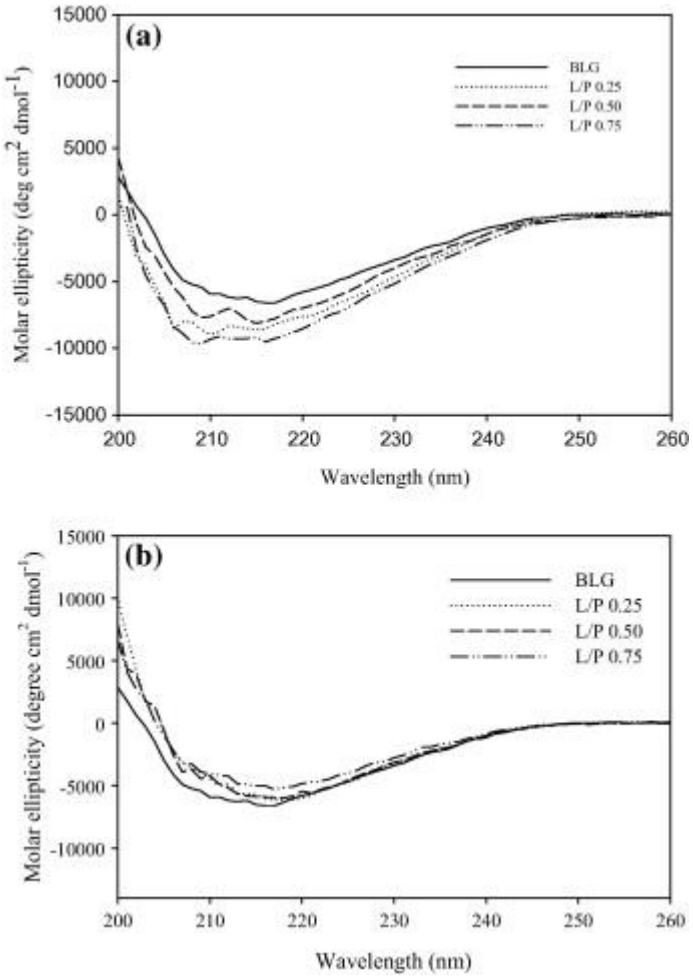

Fig. 3. Far-UV circular dichroism spectra of 13.6 μM BLG in the absence and presence of different concentrations of BDMC (a) and DABC (b) measured in 0.050 M phosphate buffer pH 6.4.

Table 2. Content of the secondary structure of BLG upon interaction with BDMC (a) and DABC (b) in different molar ratios of ligand to protein measured in 0.05 M phosphate buffer pH 6.4, and [BLG] = 13.6 μM.

Ligand to protein molar ratios	**BDMC**			**DABC**		
	α-Helix (%)	**β-Sheet (%)**	**Random coil (%)**	**α-Helix (%)**	**β-Sheet (%)**	**Random coil (%)**
0	19.6	41.4	39.0	19.6	41.4	39.0

Ligand to protein molar ratios	BDMC			DABC		
	α-Helix (%)	β-Sheet (%)	Random coil (%)	α-Helix (%)	β-Sheet (%)	Random coil (%)
0.25	25.3	38.9	35.8	22.6	38.8	38.6
0.50	24.0	39.1	36.9	21.2	39.8	39.0
0.75	29.2	36.9	33.9	18.5	41.6	39.9

The near-UV and visible range CD spectra (260–550) in addition to the far-UV region, were investigated in the presence of BDMC and DABC. The induced CD spectra are presented in Fig. 4. BDMC and DABC are achiral molecules and do not exhibit any CD spectra. The optical activities shown in this figure indicate the well-known phenomenon of protein-induced chirality which arises from conformational adaptation to the asymmetric protein binding sites. This phenomenon can also be caused by interaction between ligand molecules held in chiral arrangement relative to each other by the protein sites. Consequently, being bound to the protein, BDMC and DABC behave as chiral molecules and exhibit optical activities.

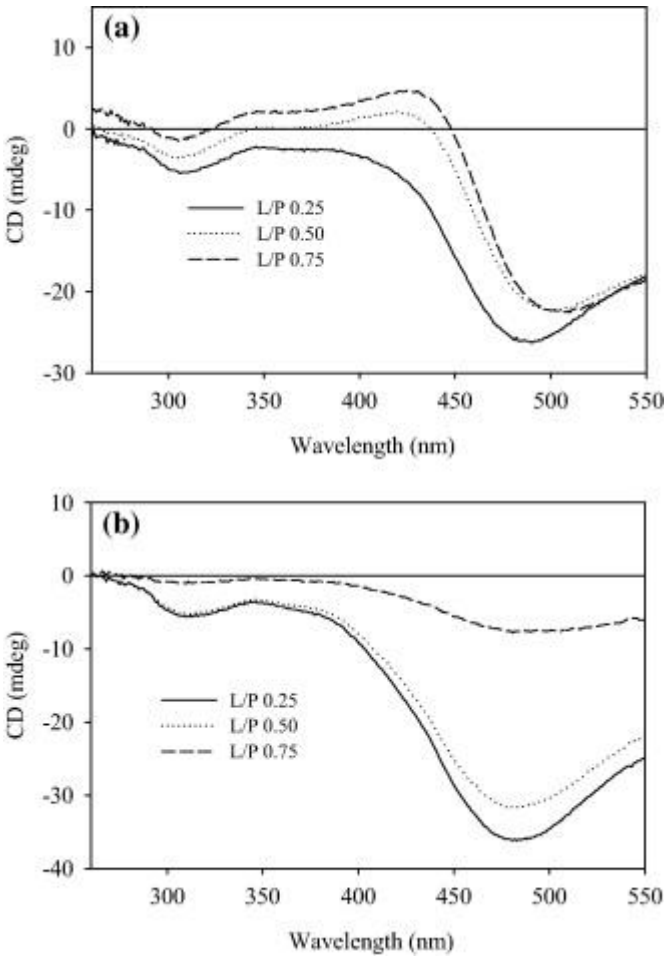

Fig. 4. Induced CD spectra of BLG complex with BDMC (a) and DABC (b) measured in 0.050 M phosphate buffer pH 6.4 and [BLG] = 57 μM.

Fig. 4a shows a strong negative *Cotton* band centered at 496 nm and a very weak negative *Cotton* band at 308 nm in 0.25 M ratio of BDMC to BLG. The intensity of the negative *Cotton* band at 496 nm decreased in 0.5 M ratios L/P and shifted to longer wavelength (500 nm) and another weak positive *Cotton* band at 420 nm appeared. The intensity of this positive band increases in 0.75 L/P solution and shifted slightly to longer wavelengths (425 nm) and the intensity of the negative *Cotton* band decreased and shifted to 510 nm wavelength.

Fig. 4b shows a strong negative *Cotton* band centered at 480 nm due to the interaction of the DABC with BLG. The intensity of this negative band is significantly decreased by increasing the concentration of DABC.

The cotton effects in the induced CD spectra indicated that the chiral configuration and orientation of BDMC and DABC which are imposed by the asymmetric protein binding site are different for these two curcuminoids. This result may be related to the different affinities of BDMC and DABC toward BLG.

Molecular docking studies

BLG consists of a single polypeptide chain of 162 amino acid residues and has a three-dimensional structure consisting of one α-helix and nine anti-parallel β-strands with eight β-sheets folded into a cone-shaped barrel forming a hydrophobic pocket [3]. As discussed in the energy transfer section (Section 'Energy transfer between BLG and BDMC'), two main binding sites of BLG are the central hydrophobic calyx and the surface cleft. Polar aromatic compounds, such as *p*-nitrophenyl phosphate, 5-fluorocytosine, ellipticine and protoporphyrin, bind to the outer surface site [64], [65].

In this study, the molecular docking program ArgusLab 4.0.1 program was chosen for examining the binding mode of BDMC and DABC at the active site of BLG. The docking results showed that BDMC and DABC bind to the surface of the protein by four and one hydrogen bond interactions, respectively (Fig. 5).

(a)

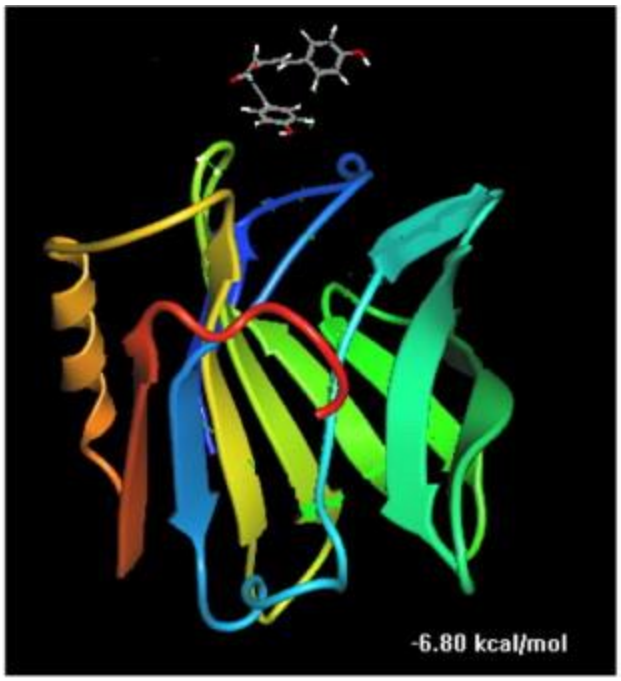

(b)

Fig. 5. BDMC (a) and DABC (b) docked in the surface of BLG using ArgusLab 4.0.1. Ligands, depicted in a stick model (light gray), and BLG, represented in cartoon ribbon.

There are four hydrogen bonds between BDMC and Arg(124), Asp(129), Glu(131) and Lys(101) of BLG with distances of 1.9 Å, 2.1 Å, 1.9 Å and 1.8 Å, respectively (Fig. 6a). Also there is one hydrogen bond between DABC and Asp (129) of BLG, with a distance of 1.8 Å (Fig. 6b).

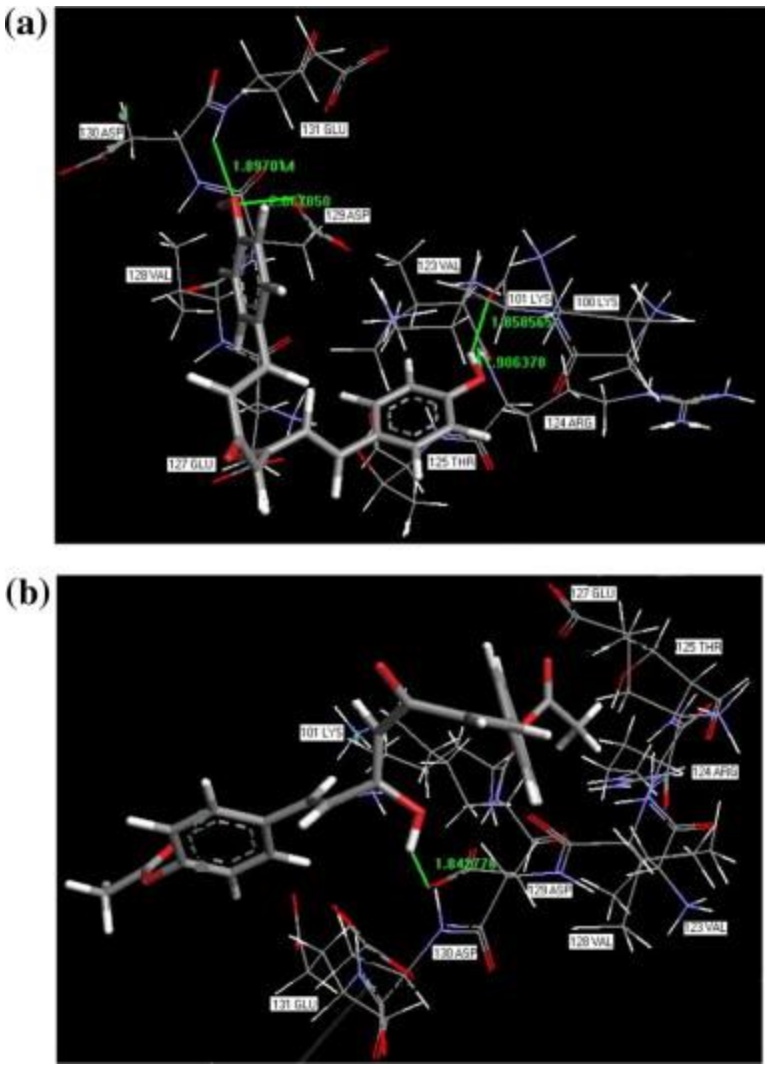

Fig. 6. The docking poses of the BLG-BDMC (a) and BLG-DABC (b) complex. Ligands are rendered as cylinders. H-bonds (as highlighted by the line in green colors) formed between ligands and BLG. (For interpretation of the references to colour in this figure legend, the reader is referred to the web version of this article.)

Thus it can be concluded that the interaction of BDMC and DABC with BLG is not mainly hydrophobic and the phenolic OH groups in the structure of BDMC which are acetylated in DABC have a significant role in the binding process. These results are in perfect agreement with the results obtained from fluorescence emission (see Section 'Fluorescence studies of BLG quenched by BDMC and DABC').

The binding constant for BDMC-BLG and DABC-BLG were about $9.7 \times 10^4\ M^{-1}$ and $2.8 \times 10^2\ M^{-1}$, respectively. Also, the free energy change, $\Delta G°$, for the binding of BDMC and DABC to BLG were about -6.8 kcal mol^{-1} and -3.35 kcal mol^{-1}, respectively. The above results closely matched the experimental data, which gave binding constants and free energy values of $8.99 \pm 0.1 \times 10^4\ M^{-1}$ and 6.75 kcal mol^{-1}, respectively, for BDMC and $1.87 \pm 0.1 \times 10^2\ M^{-1}$ and 3.10 kcal mol^{-1}, respectively, for DABC.

Therefore, the results of molecular docking indicate that the interaction between these ligands and BLG are dominated by hydrogen bonds which is in agreement with fluorescence data. It was important to note that the Trp-19 residue of BLG is in close proximity of the ligands molecule. This finding provides a good structural basis to explain the efficient fluorescence quenching of BLG emission in the presence of BDMC and DABC. Our results have shown that BDMC and DABC can interact with BLG in surface cleft with hydrogen bonding interaction which is in consistent with previously published data on other ligand molecules [62], [63], [64], [65].

Analysis of the dynamics trajectories

The trajectories were stable during the whole production part of the 10,000 ps MD simulation run. The trajectory stability was checked and was corroborated by the analysis of root mean square deviations (RMSDs) of back bone atoms of protein as functions of time for the BLG and its complexes with BDMC and DABC (Fig. 7). The RMSD of back bone atoms steadily increased and then stabilized around 2 ns and remained stable till the end of the simulation indicating that the molecular system was well behaved thereafter. The rmsd values of atoms in BLG and BLG–ligand complexes were calculated from a 2000 to 10,000 ps trajectory, where the data points were fluctuated for BLG, BLG-BDMC and BLG-DABC in about 0.22 ± 0.011 nm, 0.15 ± 0.015 nm and 0.22 ± 0.014 nm, respectively.

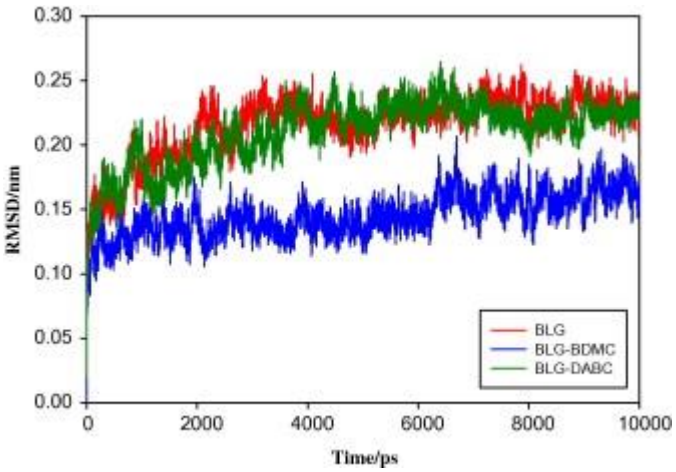

Fig. 7. rmsd values for unliganded BLG and BLG-ligand complexes during 10,000 ps MD simulation using GROMACS 4.5.6 package.

Fig. 8 shows the radius of gyration (R_g) values of unliganded BLG and BLG–ligand complexes. Stabilizing of the R_g values in these systems at about 1500 ps, indicates that the MD simulation achieved equilibrium after 1500 ps. Initial R_g values of the unliganded BLG and BLG–ligand complexes were 1.44 nm. The unliganded BLG, BLG-BDMC and BLG-DABC were stabilized at 1.40 ± 0.006 nm, 1.43 ± 0.005 nm and 1.40 ± 0.007 nm, respectively (Fig. 8). The present MD simulation is in good agreement with the earlier experimental report for the R_g value of BLG (1.39 ± 0.04 nm) [66].

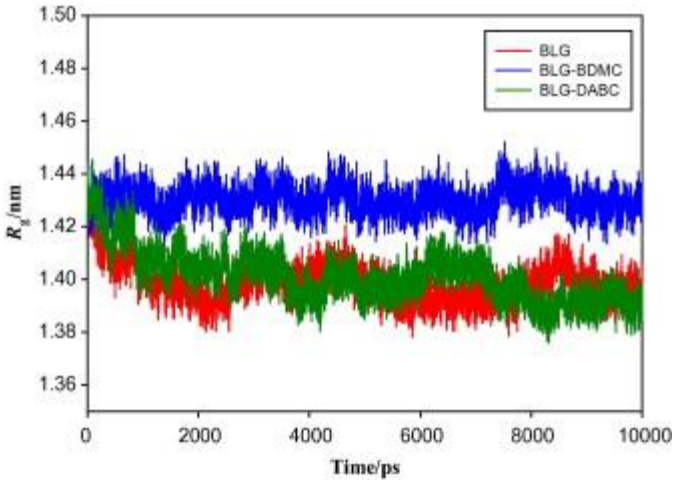

Fig. 8. Time evolution of the radius of gyration (R_g) during 10,000 ps of MD simulation of BLG and BLG-ligands complexes using GROMACS 4.5.6 package and the GROMOS96 43a1 force field at 300 K and 1 bar.

The above results indicated that the radius of gyration value increases about 2.5% upon BDMC complexation and does not change tangibly upon the DABC complexation with respect to free BLG. This clearly indicates that the binding of the DABC to BLG does not lead to the conformational changes in the BLG during MD simulation. However, BDMC changes the microenvironment of BLG and causes for the change of BLG conformation. It can be clearly seen that the radius of gyration of BLG increases upon binding of the BDMC implying a less compact structure after the simulation. These results are in coincidence with the experimental CD data shown in Table 2.

The root mean square fluctuation (rmsf) plots of free BLG and BLG-ligand complexes are shown in Fig. 9. The rmsf's were plotted against residue numbers based on the 10,000 ps trajectory in this figure. The profiles of atomic fluctuations were found to be very similar to those of BLG and BLG–ligand complexes. Our results clearly indicate that the residues in surface cleft have low fluctuations and it can be judged that the structure of ligand binding site remains approximately rigid during the simulation.

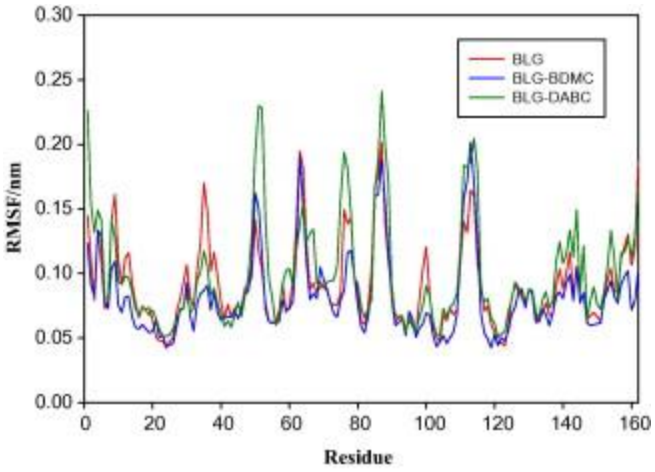

Fig. 9. The rmsf values of unliganded BLG and BLG-ligands complexes were plotted against residue numbers. The results are based on the 10,000 ps trajectory.

Conclusion

This study demonstrates the interaction of BDMC as one of the bioactive constituents of turmeric and DABC as a novel synthetic curcuminoid with the lipocalin member bovine β-lactoglobulin (BLG) genetic variant B as an important carrier of several physiological relevant ligands. Fluorescence quenching results represented that BDMC and DABC bind to BLG with binding constants of $8.99 \pm 0.1 \times 10^4\ M^{-1}$ and $1.87 \pm 0.1 \times 10^2\ M^{-1}$, respectively. These binding constants gave free energy values of -6.75 kcal mol^{-1} and -3.10 kcal mol^{-1} for BDMC and DABC, respectively. The analysis of CD spectra represented an increasing in the α-helix content of BLG with a decreasing trend of the random coil and the β-sheet contents in the presence of BDMC, while, there is no significant change in the secondary structure contents of BLG due to the interaction with DABC. These results reflect the stronger interaction with BDMC than DABC which is in consistent with the fluorescence quenching and molecular docking results.

The molecular docking studies indicated that the BDMC and DABC bind to the surface cleft of BLG, with four and one hydrogen bonding interactions, respectively. These results suggested the key role of OH groups in the binding of curcuminoids to BLG. MD simulation studies revealed that BLG and BLG–ligand complexes were stabilized around 1500 ps and also exhibited conformational changes during BDMC binding to BLG. Although, the binding of DABC did not change the conformation of BLG. Also, the profiles of atomic fluctuations showed that the structure of ligand binding site remains approximately rigid during the simulation.

Acknowledgment

The financial support of Research Council of University of Isfahan is gratefully acknowledged.

References

[1] D.R. Flower, A.C. North, C.E. Sansom, The lipocalin protein family: structural and sequence overview, Biochim. Biophys. Acta 1482 (2000) 9–24.

[2] S. Schlehuber, A. Skerra, Lipocalins in drug discovery: from natural ligandbinding proteins to ‘anticalins’, Drug Discovery Today 10 (2005) 23–33.

[3] L. Sawyer, G. Kontopidis, The core lipocalin, bovine b-lactoglobulin, Biochim. Biophys. Acta 1482 (2000) 136–148.
[4] A. Dong, J. Matsuura, S.D. Allison, E. Chrisman, M.C. Manning, J.F. Carpenter, Infrared and circular dichroism spectroscopic characterization of structural differences between b-lactoglobulin A and B, Biochemistry 35 (1996) 1450–1457.
[5] S. Brownlow, J.H.M. Cabral, R. Cooper, D.R. Flwoer, S.J. Yewdall, I. Polikarpov, A.C.T. North, L. Sawyer, Bovine [beta]-lactoglobulin at 1.8 Å resolution-still an enigmatic lipocalin, Structure 5 (1997) 481–495.
[6] G. Kontopidis, C. Holt, L. Sawyer, The ligand-binding site of bovine [beta]-lactoglobulin: evidence for a function?, J Mol. Biol. 318 (2002) 1043–1055.
[7] G. Kontopidis, C. Holt, L. Sawyer, [beta]-Lactoglobulin: binding properties, structure, and function, J. Dairy Sci. 87 (2004) 785–796.
[8] S.Y. Wu, M.D. Pérez, P. Puyol, L. Sawyer, b-Lactoglobulin binds palmitate within its central cavity, J. Biol. Chem. 274 (1999) 170–174.
[9] A. Goel, A.B. Kunnumakkara, B.B. Aggarwal, Curcumin as ‘‘Curecumin’’: from kitchen to clinic, Biochem. Pharmacol. 75 (2008) 787–809.
[10] R.A. Sharma, A.J. Gescher, W.P. Steward, Curcumin: the story so far, Eur. J. Cancer 41 (2005) 1955–1968.
[11] G.K. Jayaprakasha, L. Jagan Mohan Rao, K.K. Sakariah, Chemistry and biological activities of C. longa, Trends Food Sci. Technol. 16 (2005) 533–548.
[12] C.A.C. Araújo, L.L. Leon, Biological activities of Curcuma longa L., Mem Inst. Oswaldo Cruz 96 (2001) 723–728.
[13] F. Kiuchi, Y. Goto, N. Sugimoto, N. Akao, K. Kondo, Y. Tsuda, Nematocidal activity of turmeric: synergistic action of curcuminoids, Chem. Pharm. Bull. 41 (1993) 1640–1643.
[14] P. Limtrakul, S. Lipigrongoson, O. Namwong, A. Apisariyakul, F.W. Dunn, Inhibitory effect of dietary curcumin on skin carcinogenesis in mice, Cancer Lett. 116 (1997) 197–203.
[15] P. Limtrakul, S. Anuchapreeda, S. Lipigrongoson, F.W. Dunn, Inhibition of

carcinogen induced c-Ha-ras and c-fos proto-oncogenes expression by dietary curcumin, BMC Cancer 1 (2001) 1–7.
[16] T. Masuda, K. Hidaka, A. Shinohara, T. Maekawa, Y. Takeda, H. Yamaguchi, Chemical studies on antioxidant mechanism of curcuminoid: analysis of radical reaction products from curcumin, J. Agric. Food Chem. 47 (1999) 71–77.
[17] R.M.N. Sreejayan, Nitric oxide scavenging by curcuminoids, J. Pharm. Pharmacol. 49 (1997) 105–107.
[18] S. Singh, B.B. Aggarwal, Activation of transcription factor NF-jB is suppressed by curcumin (diferuloylmethane), J. Biol. Chem. 270 (1995) 24995–25000.
[19] S. Aggarwal, H. Ichikawa, Y. Takada, S.K. Sandur, S. Shisdodia, B.B. Aggarwal, Curcumin (diferuloylmethane) down-regulates expression of cell proliferation and antiapoptotic and metastatic gene products through suppression of IjBa kinase and Akt activation, Mol. Pharmacol. 69 (2006) 195–206.
[20] M.K. Bae, S.H. Kim, J.W. Jeong, Y.M. Lee, H.S. Kim, S.R. Kim, I. Yun, S.K. Bae, K.W. Kim, Curcumin inhibits hypoxia-induced angiogenesis via down-regulation of HIF-1, Oncol. Rep. 15 (2006) 1557–1562.
[21] P. Limtrakul, S. Anuchapreeda, D. Buddhasukh, Modulation of human multidrug-resistance MDR-1 gene by natural curcuminoids, BMC Cancer 4 (2004) 1–6.
[22] P. Limtrakul, Curcumin as a chemosensitizer, Adv. Exp. Med. Biol. 595 (2007) 269–300.
[23] S. Yodkeeree, W. Chaiwangyen, S. Garbisa, P. Limtrakul, Curcumin, demethoxycurcumin and bisdemethoxycurcumin differentially inhibit cancer cell invasion through the down-regulation of MMPs and uPA, J. Nutr. Biochem. 20 (2009) 87–95.
[24] A.J. Ruby, G. Kuttan, B.K. Dinesh, K.N. Rajasekharan, R. Kuttan, Anti-tumour and antioxidant activity of natural curcuminoids, Cancer Lett. 94 (1995) 79–83.
[25] S.I. Hoehle, E. Pfeiffer, A.M. Sólyom, M. Metzler, Metabolism of curcuminoids in tissue slices and subcellular fractions from rat liver, J. Agric. Food Chem. 54 (2006) 756–764.

[26] L.Y. Guo, X.F. Cai, J.J. Lee, S.S. Kang, E.M. Shin, H.Y. Zhou, J.W. Jung, Y.S. Kim, Comparison of suppressive effects of demethoxycurcumin and bisdemethoxycurcumin on expressions of inflammatory mediators In Vitro and In Vivo, Arch. Pharm. Res. 31 (2008) 490–496.
[27] T. Matsunaga, S. Endo, M. Soda, H.T. Zhao, O. El-Kabbani, K. Tajima, A. Hara, Potent and selective inhibition of the tumor marker AKR1B10 by bisdemethoxycurcumin: probing the active site of the enzyme with molecular modeling and site-directed mutagenesis, Biochem. Biophys. Res. Commun. 389 (2009) 128–132.
[28] K. Mohammadi, K.H. Thompson, B.O. Patrick, T. Storr, C. Martins, E. Polishchuk, V.G. Yuen, J.H. McNeill, C. Orvig, Synthesis and characterization of dual function vanadyl, gallium and indium curcumin complexes for medicinal applications, J. Inorg. Biochem. 99 (2005) 2217–2225.
[29] F. Mehranfar, A.K. Bordbar, N. Fani, M. Keyhanfar, Binding analysis for interaction of diacetylcurcumin with b-casein nanoparticles by using fluorescence spectroscopy and molecular docking calculations, Spectrochim. Acta, Part A 115 (2013) 629–635.
[30] F. Mehranfar, A.K. Bordbar, M. Keyhanfar, M. Behbahani, Spectrofluoremetric and molecular docking study on the interaction of bisdemethoxycurcumin with bovine b-casein nanoparticles, J. Lumin. 143 (2013) 687–692.
[31] F. Mohammadi, A.K. Bordbar, K. Mohammadi, A. Divsalar, A.A. Saboury, Circular dichroism and fluorescence spectroscopic study on the interaction of bisdemethoxycurcumin and diacetylbisdemethoxycurcumin with human serum albumin, Can. J. Chem. 88 (2010) 155–163.
[32] E. Dufour, T. Haertle, Binding of retinoids and [beta]-carotene to [beta]-lactoglobulin. Influence of protein modifications, Biochim. Biophys. Acta 1079 (1991) 316–320.
[33] P. Manavalan, W.C.J.R. Johnson, Variable selection method improves the prediction of protein secondary structure from circular dichroism spectra, Anal. Biochem. 167 (1987) 76–85.
[34] J.T. Yang, C.S.C. Wu, H.M. Martinez, Calculation of protein conformation from

circular dichroism, Methods Enzymol. 130 (1986) 208–269.
[35] E. Dufour, P. Robert, D. Bertrand, T. Haertlé, Conformation changes of blactoglobulin: an ATR infrared spectroscopic study of the effect of pH and
ethanol, J. Protein Chem. 13 (1994) 143–149.
[36] M.A. Thompson, ArgusLab 4.0, Planaria Software LLC, Seattle, 2004, http:// www.ArgusLab.com.
[37] M.A. Thompson, Molecular docking using ArgusLab: an efficient shape-based search algorithm and the AScore scoring function. Poster presentation, Fall ACS meeting, Philadelphia, 2004.
[38] K. Nikolic, S. Filipic, D. Agbaba, QSAR study of imidazoline antihypertensive drugs, Bioorg. Med. Chem. 16 (2008) 7134–7140.
[39] M.W. Schmidt, K.K. Baldridge, J.A. Boatz, S.T. Elbert, M.S. Gordon, J.H. Jensen, S. Koseki, N. Matsunaga, K.A. Nguyen, S.J. Su, T.L. Windus, M. Dupuis, J.A. Montgomery, General atomic and molecular electronic structure system, J. Comput. Chem. 14 (1993) 1347–1363.
[40] H.J.C. Berendsen, D. Van der Spoel, R. Van Drunen, GROMACS: a messagepassing parallel molecular dynamics implementation, Comput. Phys. Commun. 91 (1995) 43–56.
[41] E. Lindah, B. Hess, D. Van der Spoel, GROMACS 3.0: a package for molecular simulation and trajectory analysis, J. Mol. Model. 7 (2001) 306–317.
[42] W.F. Van Gunsteren, S.R. Billeter, A.A. Eising, P.H. Hünenberger, P.K.H.C. Krüger, A.E. Mark, W.R.P. Scott, I.G. Tironi, Biomolecular Simulation: The GROMOS96 Manual and User Guide, Vdf Hochschulverlag AG, Zürich, 1996.
[43] W.F. Van Gunsteren, X. Daura, A.E. Mark, in: P. Von Rague Schleyer (Ed.), Encyclopedia of Computational Chemistry, Wiley and Sons, Chichester, UK, 1998, p. 1211.
[44] H.J.C. Berendsen, J.P.M. Postma, W.F. Van Gunstetren, J. Hermans, in: B. Pullman (Ed.), Intermolecular Forces, Reidel, Dordrecht, The Netherlands, 1981, p. 331.
[45] A.W. Schuttelkopf, D.M.F. Van Aalten, PRODRG: a tool for high-throughput crystallography of protein–ligand complexes, Acta Crystallogr. 60 (2004)

1355–1363.
[46] J.R. Lakowicz, Principles of Fluorescence Spectroscopy, second ed., Kluwer Academic, New York, 1999.
[47] B.J. Harvey, E. Bell, L. Brancaleon, A tryptophan rotamer located in a polar environment probes pH-dependent conformational changes in bovine blactoglobulin A, J. Phys. Chem. B 111 (2007) 2610–2620.
[48] M.I. Viseu, T.I. Carvalho, S.M.B. Costa, Conformational transitions in [beta]-lactoglobulin induced by cationic amphiphiles: equilibrium studies, Biophys. J. 86 (2004) 2392–2402.
[49] L.K. Creamer, Effect of sodium dodecyl sulfate and palmitic acid on the equilibrium unfolding of bovine beta-lactoglobulin, Biochemistry 34 (1995) 7170–7176.
[50] K. Sakai, K. Sakurai, M. Sakai, M. Hoshino, Y. Goto, Conformation and stability of thiol-modified bovine [beta] lactoglobulin, Protein Sci. 9 (2000) 1719–1729.
[51] Y. Cho, C.A. Batt, L. Sawyer, Probing the retinol-binding site of bovine betalactoglobulin, J. Biol. Chem. 269 (1994) 11102–11107.
[52] W.R. Ware, Oxygen quenching of fluorescence in solution: an experimental study of the diffusion process, J. Phys. Chem. 66 (1962) 455–458.
[53] M. Jiang, M.X. Xie, D. Zheng, Y. Liu, X.Y. Li, X. Cheng, Spectroscopic studies on the interaction of cinnamic acid and its hydroxyl derivatives with human serum albumin, J. Mol. Struct. 692 (2004) 71–80.
[54] F. Mohammadi, A.K. Bordbar, A. Divsalar, K. Mohammadi, A.A. Saboury, Analysis of binding interaction of curcumin and diacetylcurcumin with human and bovine serum albumin using fluorescence and circular dichroism spectroscopy, Protein J. 28 (2009) 189–196.
[55] F. Mohammadi, A.K. Bordbar, A. Divsalar, K. Mohammadi, A.A. Saboury, Interaction of curcumin and diacetylcurcumin with the lipocalin member blactoglobulin, Protein J. 28 (2009) 117–123.
[56] S. Weiss, Fluorescence spectroscopy of single biomolecules, Science 283 (1999) 1676–1683.
[57] R.D. Fugate, P.S. Song, Spectroscopic characterization of [beta]-lactoglobulin–

retinol complex, Biochim. Biophys. Acta 625 (1980) 28–42.
[58] D.C. Lange, R. Kothari, R.C. Patel, S.C. Patel, Retinol and retinoic acid bind to a surface cleft in bovine [beta]-lactoglobulin: a method of binding site determination using fluorescence resonance energy transfer, Biophys. Chem. 74 (1998) 45–51.
[59] Y.J. Wang, M.H. Pan, A.L. Cheng, L.I. Lin, Y.S. Ho, C.Y. Hsieh, J.K. Lin, Stability of curcumin in buffer solutions and characterization of its degradation products, J. Pharm. Biomed. Anal. 15 (1997) 1867–1876.
[60] H.H. Tonnesen, J.Z. Karlsen, Studies on curcumin and curcuminoids: alkaline degradation of curcumin, Lebensm. Unters. Forsch. 180 (1985) 132–134.
[61] B.Y. Qin, M.C. Bweley, L.K. Creamer, H.M. Baker, E.N. Baker, G.B. Jameson, Structural basis of the Tanford transition of bovine b-lactoglobulin, Biochemistry 37 (1998) 14014–14023.
[62] L. Liang, H.A. Tajmir-Riahi, M. Subirade, Interaction of b-lactoglobulin with resveratrol and its biological implications, Biomacromolecules 9 (2008) 50–56.
[63] A. Taheri-Kafrani, Y. Choiset, D.A. Faizullin, Y.R. Zuev, V.V. Bezuglov, J.M. Chobert, A.K. Bordbar, T. Haertlé, Interactions of b-lactoglobulin with serotonin and arachidonyl serotonin, Biopolymers 95 (2011) 871–880.
[64] L. Sawyer, P.N. Barlow, M.J. Boland, L.K. Creamer, H. Denton, P.J.B. Edwards, C. Holt, G.B. Jameson, G. Kontopidis, G.E. Norris, S. Uhrínová, S.Y. Wu, Milk protein structure-what can it tell the dairy industry?, Int Dairy J. 12 (2002) 299–310.
[65] E. Dufour, M.C. Marden, T. Haertlté, [beta]-Lactoglobulin binds retinol and protoporphyrin IX at two different binding sites, FEBS Lett. 277 (1990) 223–226.
[66] D. Renard, Dissertation, Université de Nantes, Faculté des science et des techniques, France, 1994.